CHEMISTRY OF MATERIALS

Article

pubs.acs.org/cm

Wafer-Scale Growth of WSe_2 Monolayers Toward Phase-Engineered Hybrid WO_x/WSe_2 Films with Sub-ppb NO_x Gas Sensing by a Low-Temperature Plasma-Assisted Selenization Process

Henry Medina,[†] Jian-Guang Li,[†] Teng-Yu Su,[†] Yann-Wen Lan,[§] Shao-Hsin Lee,[†] Chia-Wei Chen,[†] Yu-Ze Chen,[†] Arumugam Manikandan,[†] Shin-Hung Tsai,[∥] Aryan Navabi,[∥] Xiaodan Zhu,[∥] Yu-Chuan Shih,[†] Wei-Sheng Lin,[†] Jian-Hua Yang,[†] Stuart R. Thomas,[†] Bo-Wei Wu,[†,§] Chang-Hong Shen,[§] Jia-Min Shieh,[§] Heh-Nan Lin,[†] Ali Javey,[⊥] Kang L. Wang,[§] and Yu-Lun Chueh*[,†,‡]

[†]Department of Materials Science and Engineering, National Tsing Hua University, Hsinchu 30013, Taiwan, Republic of China

[‡]School of Material Science and Engineering, State Key Laboratory of Advanced Processing and Recycling of Non-ferrous Metals, Lanzhou University of Technology, Lanzhou City 730050, Gansu, P.R. China

[§]National Nano Device Laboratories, No. 26, Prosperity Road 1, Hsinchu 30078, Taiwan, Republic of China

[∥]Department of Electrical Engineering, University of California, Los Angeles, California 90095, United States

[⊥]Electrical Engineering and Computer Sciences, University of California, Berkeley, California 94720, United States

Supporting Information

ABSTRACT: An inductively coupled plasma (ICP) process was used to synthesize transition metal dichalcogenides (TMDs) through a plasma-assisted selenization process of metal oxide (MO_x) at a temperature as low as 250 °C. In comparison with other CVD processes, the use of ICP facilitates the decomposition of the precursors at low temperatures. Therefore, the temperature required for the formation of TMDs can be drastically reduced. WSe_2 was chosen as a model material system due to its technological importance as a p-type inorganic semiconductor with an excellent hole mobility. Large-area synthesis of WSe_2 on polyimide (30 × 40 cm^2) flexible substrates and 8 in. silicon wafers with good uniformity was demonstrated at the formation temperature of 250 °C confirmed by Raman and X-ray photoelectron (XPS) spectroscopy. Furthermore, by controlling different H_2/N_2 ratios, hybrid WO_x/WSe_2 films can be formed at the formation temperature of 250 °C confirmed by TEM and XPS. Remarkably, hybrid films composed of partially reduced WO_x and small domains of WSe_2 with a thickness of ∼5 nm show a sensitivity of 20% at 25 ppb at room temperature, and an estimated detection limit of 0.3 ppb with a $S/N > 10$ for the potential development of a low-cost plastic/wearable sensor with high sensitivity.

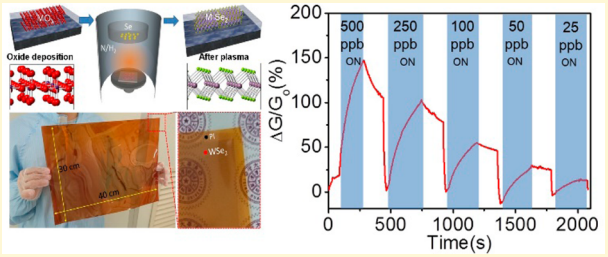

INTRODUCTION

The development and application of inorganic p-type semiconductors processed at low temperatures has been sluggish due to their poor performance (bulk hole mobilities <1 $cm^2 V^{-1} s^{-1}$) when the process temperature is lower than 500 °C.[1,2] Recently, organic p-type semiconductors have taken the lead in this field, with the development of applications including solar cells, sensors, and thin film transistors (TFTs) for low-cost flexible electronics. In particular, for sensing of oxidizing gases such as NO_x, p-type semiconductors are expected to offer better response by increasing the conductance upon gas exposure. In this regard, WSe_2 possesses a high hole mobility and a good charge transfer with NO_x molecules,[3] making it an excellent candidate as a p-type inorganic material with a thickness of below 10 nm.[4,5] Chemical vapor deposition (CVD) is a common approach used for the growth of TMDs; nevertheless, the high synthesis temperature is a major drawback for its use in flexible electronics because of the requirement of an additional transfer process.[4−7] A few studies have reported the lowest growth temperatures of 500 °C for n-type sulfur-based TMDs such as MoS_2,[8,9] while for other p-type TMDs, such as selenium-based TMDs, synthetic temperatures of below 700 °C have not yet been reported.[4−7] Although there have been reports of the synthesis of WSe_2 on an insulator directly, substrate damage caused by chalcogenide diffusion at high growth temperatures still occurs.[10] Thus, a further transfer process of the TMDs for device fabrication is needed. The transfer method is costly and inefficient for the fabrication of

Received: October 19, 2016
Revised: December 20, 2016
Published: December 21, 2016

DOI: 10.1021/acs.chemmater.6b04467
Chem. Mater. 2017, 29, 1587−1598

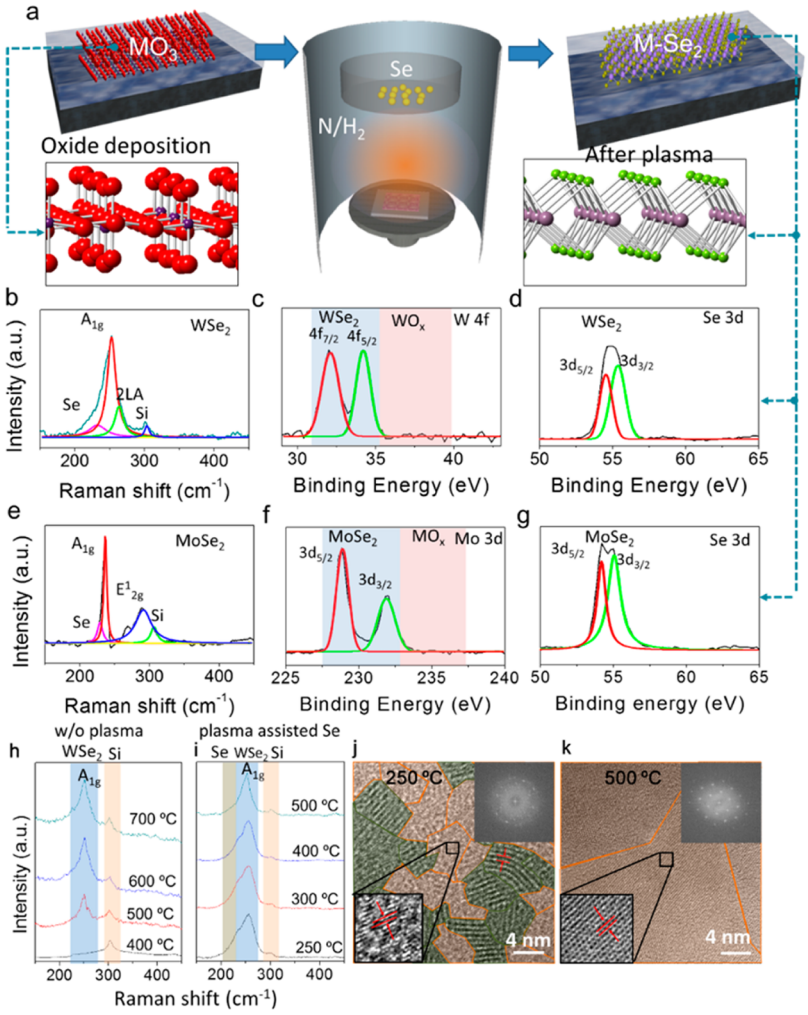

Figure 1. (a) Schematic of the low-temperature plasma-assisted selenization process. (b–d) The corresponding Raman and W-4f and Se-3d XPS spectra of WSe_2 after the plasma-assisted selenization processes of the WO_x film. (e–g) The Raman and Mo-3d and Se-3d XPS spectra of $MoSe_2$ after the plasma-assisted selenization processes of MoO_x. (h, i) Raman spectra of WO_x after the selenization process without and with the plasma treatment at different temperatures. (i, j) High-resolution plane-view TEM images of a few WSe_2 monolayers at selenization temperatures of 500 and 250 °C with plasma powers of 50 and 400 W, respectively. The upper inset shows FFT diffraction patterns. The lower inset is the zoom-in displaying the areas that have a smaller fringe pattern (~0.28 nm).

electronics over large areas due to the formation of wrinkles and scratches as well as the accumulation of polymer residues on the TMD surfaces, which leads to a degradation of the overall device performance.[11] The synthesis of TMDs with monolayers to exploit the optical properties that arise from the transition of indirect to direct bandgaps by using the conventional solid–vapor phase CVD process has been well-developed.[4−6] However, it has been reported that WSe_2 prepared with a thickness of a few monolayers offers better mobility compared to that with a monolayer.[5,12] In the standard solid–vapor growth CVD process, the most pressing difficulty lies in controlling the number of deposited TMD layers over a large area because of the uncontrolled layer formation, which leads to the formation of walls.[13,14] Instead, the predeposition of metal oxide followed by a postselenization process offers much better thickness control over a larger area and provides an easy platform that has a controllable pattern process for the direct growth of TMDs.

In this regard, we successfully demonstrate here the incorporation of an inductively coupled plasma (ICP) into a typical selenization process, which is then applied to metal oxides, namely, a plasma-assisted selenization process, for the synthesis of atomically thin TMD films at a temperature as low as 250 °C. In a comparison to other CVD processes where substrate temperature triggers the reaction between the metal oxide and the calcogen source, the use of plasma aids the decomposition of the metal oxides in the presence of high-energy Se ions facilitating the formation of TMDs at low temperature. The formation of $MoSe_2$ and WSe_2 was demonstrated by the plasma-assisted selenization process, while detailed phase and material characterizations of WSe_2 with different parameter tuning were investigated. WSe_2 was chosen as a model material system because of its technological importance as a p-type semiconductor. We have also demonstrated the large-scale synthesis of WSe_2 on 30 × 40 cm^2 polyimide and an 8-in. silicon wafer. Intrinsic hole mobilities of a few WSe_2 monolayers at different selenization temperatures were measured, reaching 40 $cm^2\ V^{-1}\ s^{-1}$ at the plasma-assisted selenization temperature of 500 °C. A hole mobility of approximately 6 $cm^2\ V^{-1}\ s^{-1}$ can be achieved at the plasma-assisted selenization temperature of 250 °C, which is a remarkable value for an inorganic p-type semiconductor to

DOI: 10.1021/acs.chemmater.6b04467
Chem. Mater. 2017, 29, 1587−1598

achieve at such a low temperature, and with a thickness of less than 5 nm. Interestingly, by controlling the ratios of the different forming gases (N_2 and H_2), a 5-nm-thick WO_x/WSe_2 hybrid structure was observed to possesses a high sensitivity to NO_x with a sensitivity over 20% at only 25 ppb, and an S/N over 40 operating at room temperature. An estimated detection limit up to 0.3 ppb at an S/N ratio larger than 10 can be achieved, which is one of the most important environmental gases to monitor contributing to the secondary formation of fine particle matter with size <2.5 μm (PM2,5).[12,13] Bending tests on the 5-nm-thick WO_x/WSe_2 hybrid structure directly synthesized on a polyimide substrate at 250 °C were demonstrated, showing a slight decrease in the sensitivity and an increase in the sheet resistance after the bending angle >75°. The plasma-assisted selenization approach toward M-Se_2 synthesis as well as hybrid MO_x/MSe_2 demonstrated here can bring major advantages in terms of performance, compatibility with traditional and next-generation flexible device processing technology, scalability, and processing cost because no further transfer process is required.

EXPERIMENTAL SECTION

Metal Oxide Deposition. RF-sputtering with WO_3 and MoO_3 targets was used under 15 mTorr in an Ar/O_2 ratio of 20 and a fixed power of 50 W. On SiO_2 and glass substrates for selenization at 500 °C, WO_x was deposited at 300 °C, while SiO_2 and PI substrates for low-temperature selenization (250 °C) were deposited at 250 °C. The time was controlled to achieve different oxide thicknesses.

Plasma-Assisted Selenization Process. After the deposition of the target metal oxide, the films were transferred to the selenization chamber. The pressure was set in the range 1−10 Torr, and the mixture of hydrogen and nitrogen inside the chamber was controlled to achieve the desired WSe_2−WO_x ratio. Then, selenium was first heated to the desired temperature of 300 °C and maintained during the entire process, while the temperature of the target substrate ramped to the desired value within 1 h. Once the temperature of the substrate is stable, the plasma is initiated for 1 h. Finally, the plasma and hydrogen flow are turned off, and the substrate and Se are left to cool naturally until the temperature decreases to below 50 °C. Then, the samples were retrieved and unloaded from the chamber.

Hall Bar Device Fabrication. In this work, we commenced the fabrication process on a few WSe_2 monolayers on a 100 mm degenerately doped n^{+2} ($N_D \sim 1 \times 10^{19}$ cm^{-3}) silicon wafer and performed a standard photolithography procedure twice, to define the Hall bar structure and contact electrodes, and subsequently, the completed WSe_2 hall bar structure was shaped by dry etching (AOE Oxide Etcher) for 5 s while contact electrodes were deposited Ti/Au (10 nm/100 nm) by standard E-beam evaporation (CHA Mark 40) at deposition rates of 0.01 nm/s for Ti and 0.1 nm/s for Au, respectively. Furthermore, a third photolithography step was performed to pattern and deposit the outside electrodes (50-nm-thick Cr/100-nm-thick Au films) that connected with the previously patterned inner electrodes. These metallic outer electrodes were in intimate contact with the inner region, allowing easy probing and biasing of the WSe_2 devices.

Fabrication of Gas Sensors and FET Devices. For the back gate devices, WSe_2 films were transferred by a polymer-assisted process onto ZrO_2, and Ti 10 nm/Pt 100 nm was later deposited by a hard mask. Gas sensor devices were fabricated directly from the as-grown film without a transfer process, but instead just by the deposition of metal electrodes by a hard mask (10 nm Cr/50 nm Au).

Characterizations. Raman spectroscopy was recorded using 514 nm laser excitation in all cases except for the PI substrate, for which Raman spectra were recorded with a 325 nm laser to avoid the strong background signal from the PI substrate measured at the laser wavelength of 514 nm. The microstructure is provided from high-resolution transmission electron microscopy (HRTEM, JEOL, JEM-3000F FEGTEM, 300 kV) with a point-to-point resolution of 017 nm equipped STEM and an energy dispersive spectrometer (EDS). The chemical bonding between tungsten and oxygen on the surface and the interior of the film were certified by X-ray photoelectron spectroscopy PHI 5000 VersaProbe II. The electrical properties of the fabricated devices were measured with a semiconductor parameter analyzer (Keithley 4200) at room temperature. An Ecopia HMS-3000 Hall measurement system was used for measurements of the resistivity, carrier concentration, and mobility of a few WSe_2 monolayers.

RESULTS AND DISCUSSION

Figure 1a describes the overall plasma-assisted selenization process from metal oxide to a few TMD monolayers. As a proof of concept, metal oxides, such as tungsten oxide (WO_x) and molybdenum oxide (MoO_x), were deposited on silicon oxide arbitrary substrates by sputtering with thicknesses 2−10 nm, followed by the plasma-assisted selenization process to form the TMDs. (See Experimental Section and Figure S1.) Figure 1b shows Raman spectra of a 5-nm-thick WO_x film after completing the plasma-assisted selenization process under a power of 50 W at 500 °C for 1 h. The spectrum was then deconvoluted into 4 peaks. The peak located at 250 cm^{-1} corresponds to an out-of-plane vibration of the selenium atoms (A_{1g}), while the peak located at 260 cm^{-1} refers to the second-order vibration of the longitudinal acoustic phonon at the M point (2LA(M)), which clearly confirms the formation of a few WSe_2 monolayers.[15] Note that the peak position of the in-plane vibrational mode (E^1_{2g}) is very close to the position of A_{1g}, which makes identification difficult.[16] The notation that expresses this mode as A_{1g} is preferred because of its stronger intensity compared to E^1_{2g} under a 532 nm excitation wavelength.[16] The peak at 300 cm^{-1} is characteristic of Si from SiO_2/Si substrates (Figure S2a and Figure S2b). Due to the particularities of our process, the deposition can be easily extended to different substrates; in order to demonstrate its feasibility, WSe_2 was synthesized on additional substrates such as silicon nitride and sapphire, as shown in Figure S2c. A small shoulder located at 235 cm^{-1} was also observed, which is most likely attributed to unreacted selenium (Se) and corresponds to crystalline Se (t-Se).[17,18] To confirm the existence of the t-Se peak, an empty glass sample was placed for a few hours under the plasma-assisted selenization process (Figure S3). X-ray photoelectron spectroscopy (XPS) was employed to further confirm the transformation of the WO_x into a few WSe_2 monolayers. Figure 1c,d presents the W 4f and Se 3d XPS spectra, respectively. The peaks located at 32.1 and 34 eV are attributed to binding energies of W $4f_{7/2}$ and $4f_{5/2}$ for a few WSe_2 monolayers, while the two peaks located at 54.5 and 55.2 eV correspond to the $3d_{5/2}$ and $3d_{3/2}$ binding energies of the Se atoms in WSe_2.[19] Similarly, the formation of $MoSe_2$ was also demonstrated and confirmed by the associated Raman spectra (Figure 1e), where the characteristic modes A_{1g} (241 cm^{-1}) and E^1_{2g} (290 cm^{-1}) from $MoSe_2$ can be clearly observed.[20] The Mo 3d spectra display two peaks at 229 and 232 eV, which correspond to binding energies of Mo $3d_{5/2}$ and $3d_{3/2}$ in $MoSe_2$ (Figure 1f). In the case of the Se 3d spectra, the corresponding $3d_{5/2}$ (54.4 eV) and $3d_{3/2}$ (55.3 eV) binding energies for Se in $MoSe_2$ are also present, as shown in Figure 1g.[21] No peaks were detected in the ranges 35−39 and 233−237 eV, which correspond to the binding energies of WO_x[19] and MoO_x,[22] thus implying the full transformation of WO_x and MoO_x into a few WSe_2 and $MoSe_2$ monolayers after the plasma-assisted selenization process.

DOI: 10.1021/acs.chemmater.6b04467
Chem. Mater. 2017, 29, 1587−1598

To demonstrate plasma-assisted selenization at low temperatures, we focus on optimizing the growth parameters through the formation of a few WSe_2 monolayers as the model material system. To confirm the effectiveness of the plasma-assisted process, the selenization was conducted with and without the plasma treatment. Initially, WO_x was first deposited. Subsequently, Se powder in the chalcogenide heater was set at 300 °C to provide the Se vapor that is necessary for the subsequent selenization step, and the selenization temperature (substrate temperature) was tuned from 700 to 400 °C without the plasma treatment, as shown in Figure 1h. At selenization temperatures of 700 and 600 °C, the Raman spectra show a strong A_{1g} vibrational mode, which corresponds to the WSe_2 signal, while the intensity decreases as the temperature drops to 500 °C and disappears completely at temperatures below 400 °C. It can be expected that the ionization of Se atoms into Se radicals, which have a much higher chemical reactivity, triggers the selenization via the replacement of existing oxygen by Se atoms, thus leading to a decrease in the selenization temperature during the plasma treatment. Although a "remote" concept has been applied in our plasma-assisted process, higher plasma power could still result in crystalline defects, which have also been observed during the synthesis of graphene.[23] A trade-off condition was then imposed to achieve the lowest selenization temperature within a suitable plasma power, while obtaining the complete transformation of TMDs from metal oxides with the least amount of damage to the structure due to plasma bombardment. The complete transformation of the WSe_2 monolayers from the WO_x films has been carefully tuned with different selenization temperatures accompanied by different applied plasma powers, as shown in Table 1 and Figure 1i. Interestingly, the lowest selenization temperature can be brought down to 250 °C with a plasma power of 400 W for which the WSe_2 phase remains, confirmed by the existence of a prominent A_{1g} peak (Figure 1i). Because no clear A_{1g} peak of WSe_2 was observed as the selenization temperature was below 250 °C, we believe that 250 °C is the lowest temperature that can achieve the WSe_2 phase, with no lower-temperature synthesis reported in all of the TMD literature. To analyze the crystalline quality of a few WSe_2 monolayers, the planar view high-resolution TEM images of a few WSe_2 monolayers prepared at the selenization temperatures of 250 and 500 °C with plasma powers of 400 and 50 W are shown in Figure 1j,k, respectively. For a few WSe_2 monolayers prepared at 250 °C (Figure 1j), small domains of ∼3−13 nm were observed, where the interspacing of ∼0.28 nm, corresponding to the (010) plane of WSe_2, can be indexed.[24] Those with a larger internal spacing of ∼0.69 nm are in agreement with the (001) plane of WSe_2, as marked as the green areas, which indicates the occurrence of different stacking orientations.[17] The ring pattern in the FFT diffraction pattern, as shown in the upper inset, confirms the polycrystalline feature of a few WSe_2 monolayers. A larger grain of ∼18−32 nm can be achieved once the selenization temperature increases to 500 °C with a reduced plasma power of 50 W, as shown in Figure 1k, and the corresponding FFT diffraction pattern shows symmetry spots with a [001] zone axis and confirms the larger grains of a few WSe_2 monolayers where the internal spacing of ∼0.28 nm, which corresponds to the (010) place of WSe_2, is indexed. In addition, Figure S4 displays corresponding low-magnification TEM images of a few WSe_2 monolayers that were synthesized at the plasma-assisted selenization temperatures of 250 and 500 °C. There are no major differences with the high-magnification TEM images displaying small domains that have random orientations at 250 °C, and for the 500 °C, the large domains are clearly observed. As a result, the average grain sizes of ∼8 and ∼25 nm for WSe_2 with 250 and 500 °C selenization temperatures with different powers were estimated by taking more than 10 regions in TEM images.

Table 1. Plasma Power vs. Process Temperature

temp	plasma power (W)
500	50
400	150
300	300
100	400

To further investigate the influence of the plasma power on the obtained Raman spectra, 5−7-nm-thick WO_x films were exposed to different plasma powers at the selenization temperature of 250 °C (substrate temperature), while the Se heater and selenization time were fixed at 300 °C and 1 h, respectively (Figure S5a). Note that the intensity of WSe_2 was compared to the Raman spectra at ∼300 cm^{-1}, which was contributed from Si as a reference, and the full width at the half-maximum (FWHM) of each peak was measured at different points (Figure S5b,c). The intensity ratio of A_{1g}/Si increases from 2 to 5.9 with the increased power from 200 to 400 W, while a constant increase in the average fwhm of the A_{1g} with a standard deviation (av 20 cm^{-1} to 30 cm^{-1}/std dev ∼1−4 cm^{-1}) was also observed. The increase in the A_{1g}/Si implies a greater reduction barrier of WO_x into WSe_2 during the selenization at low temperatures, which is associated with the plasma treatment. The increase in the fwhm in A_{1g} is also an indication of material damage caused by strong plasma irradiation. The corresponding cross-sectional TEM (XTEM) images at different plasma powers at the fixed selenization temperature of 250 °C are shown in Figure 2a−c. At a plasma power of 200 W, no discernible layered structure was observed, and the structure of the film is mainly amorphous (Figure 2a). Interestingly, after the plasma power increases to 300 W, two different layers were clearly differentiated, including a layered structure at the top region with an interlayer spacing of 0.69 nm, which is in agreement with the interlayer spacing of WSe_2 and an amorphous structure located at the bottom region (Figure 2b). Figure S6 presents the EDS spectra and chemical compositions at different positions marked in Figure 2b. The atomic ratios of Se with respect to W being ∼2:1 at points 1, 2, and 3 located in layered structures confirm the WSe_2 phase, while it is greatly reduced at the bottom due to the coexistence of WO_x and WSe_2. When the power was further increased to 400 W, only the layered structure with an interlayer distance of 0.69 nm can be observed as a confirmation of the complete reduction of the WO_x into WSe_2 (Figure 2c). Another advantage of our method is the precise control of the number of WSe_2 layers, depending on the initial thickness of the WO_x films. For example, a 5−7-nm-thick WO_x layer can form 6−8 WSe_2 monolayers (Figure 2d,e), while 4−5 WSe_2 monolayers were achieved as the thickness of the WO_x decreases to 4−5 nm (Figure 2f,g). However, we found that the growth of the WO_x film on the SiO_2 substrates shows a tendency to form islands rather than thin film growth once the thickness of the WO_x layer decreases below 2 nm because of the high surface energy difference or higher surface roughness between WO_x and SiO_2, which yields discontinuity in a few WSe_2 monolayers

DOI: 10.1021/acs.chemmater.6b04467
Chem. Mater. 2017, 29, 1587−1598

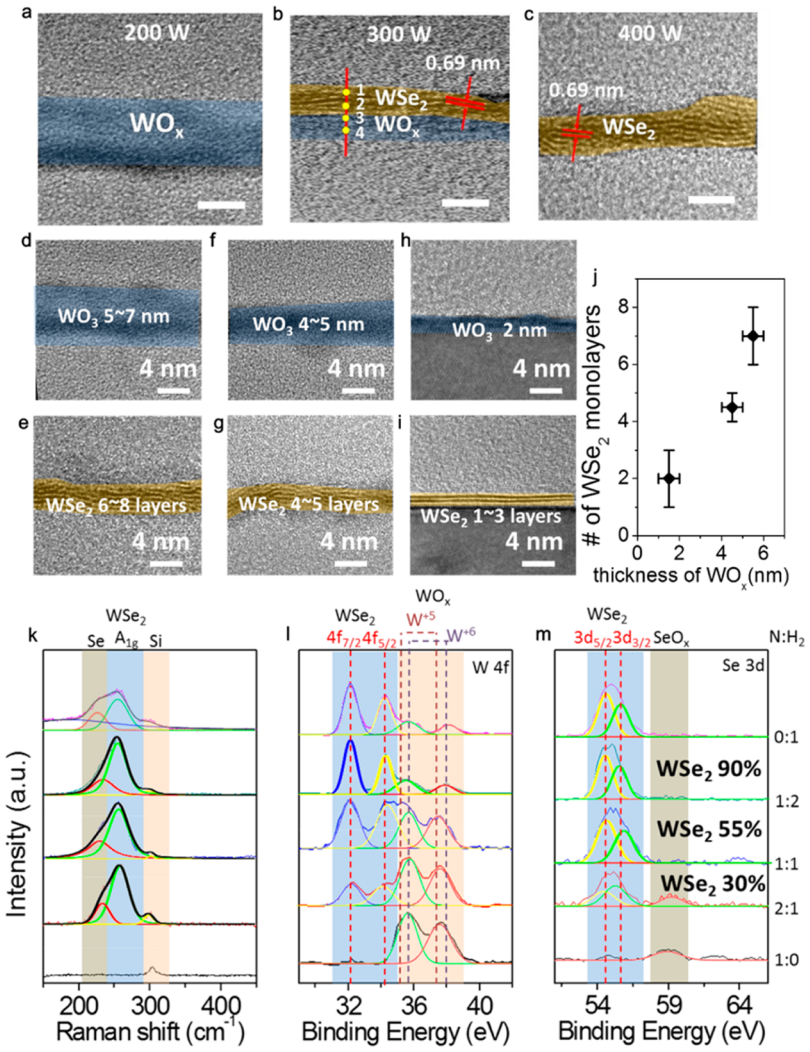

Figure 2. Cross-sectional TEM images of 5−7-nm-thick WO_x films exposed to the plasma powers of (a) 200 W, (b) 300 W, and (c) 400 W with the selenization temperature of 250 °C. (d, f, and h) Cross-sectional TEM images of as-deposited WO_x films with different thicknesses on SiO_2/Si (d and f) and sapphire (h) substrates. Parts e, g, and i show the corresponding cross-sectional TEM images of a few WSe_2 monolayers after the plasma-assisted selenization process. (j) Plot of numbers of WSe_2 layers as a function of the thicknesses of WO_x films after the plasma-assisted selenization process. In parts k, l, and m are the Raman and W 4f and Se 3d spectra of WSe_2 reduced at 250 °C and 400 W under different nitrogen and hydrogen ratios.

(Figure S7a,b). A continuous WO_x layer of ∼2 nm thickness can be achieved on a sapphire substrate because it has a significantly lower surface energy difference or a small surface roughness, which results in ∼1−3 WSe_2 monolayers (Figure 2h,i). Figure 2j summarizes the dependence of the resulting numbers of WSe_2 monolayers compared to the thicknesses of the as-deposited WO_x films. We believe that a WSe_2 monolayer is achievable as long as we can deposit very thin and uniform WO_3 by other methods such as atomic layer deposition,[25] molecular beam epitaxy,[26] and pulsed laser deposition.[27] However, in this work, we demonstrated WSe_2 devices that were prepared by films composed of a few monolayers rather than a monolayer film due to their improved mobility.[5,12] The precise thickness controllability provides different absorption abilities at different wavelengths (Figure S8)

In addition, the gas forming ratios also play a major role during the plasma-assisted selenization process. Figure 2k−m shows the Raman and W 4f and Se 3d XPS spectra of the WO_x films under the plasma-assisted selenization process at different forming gas ratios consisting of N_2 and H_2, respectively. Under a pure nitrogen atmosphere, no WSe_2 can be formed, as confirmed by Raman spectra. From the W 4f spectra of XPS, 4 peaks can be deconvoluted in accordance with the W^{6+} (38.2 and 35.5 eV) and W^{5+} (37.5 and 34.9 eV) oxidation states as expected due to the amorphous phase of the WO_x deposited by physical evaporation methods.[28] The Se 3d spectra show a small peak located at 59 eV, which corresponds to an oxidation state for Se due to residual unreacted selenium oxidized during the preparation process of the XPS samples.[29] Once a small amount of H_2 increases, the typical W $4f_{7/2}$ and $4f_{5/2}$ bands, and Se $3d_{5/2}$ and $3d_{3/2}$ bands, can be found, indicating that the selenization of WO_x obviously occurs (Figure 2l,m). To evaluate the selenization percentage of WO_x to WSe_2, the W $4f_{7/2}$ and $4f_{5/2}$ bands are further fitted using Gaussian peaks, and the areas under the curves are compared to that of the fitting of the W^{6+} and W^{5+} oxidation states of WO_x. For easy understanding, we define the ratio between the areas as the conversion percentage from the WO_x into WSe_2 as the sum of the area corresponding to W $4f_{7/2}$ and W $4f_{5/2}$ peaks of WSe_2 ($A_{W4f7/2}$ + $A_{W4f5/2}$) over the total area of the tungsten spectra

DOI: 10.1021/acs.chemmater.6b04467
Chem. Mater. 2017, 29, 1587−1598

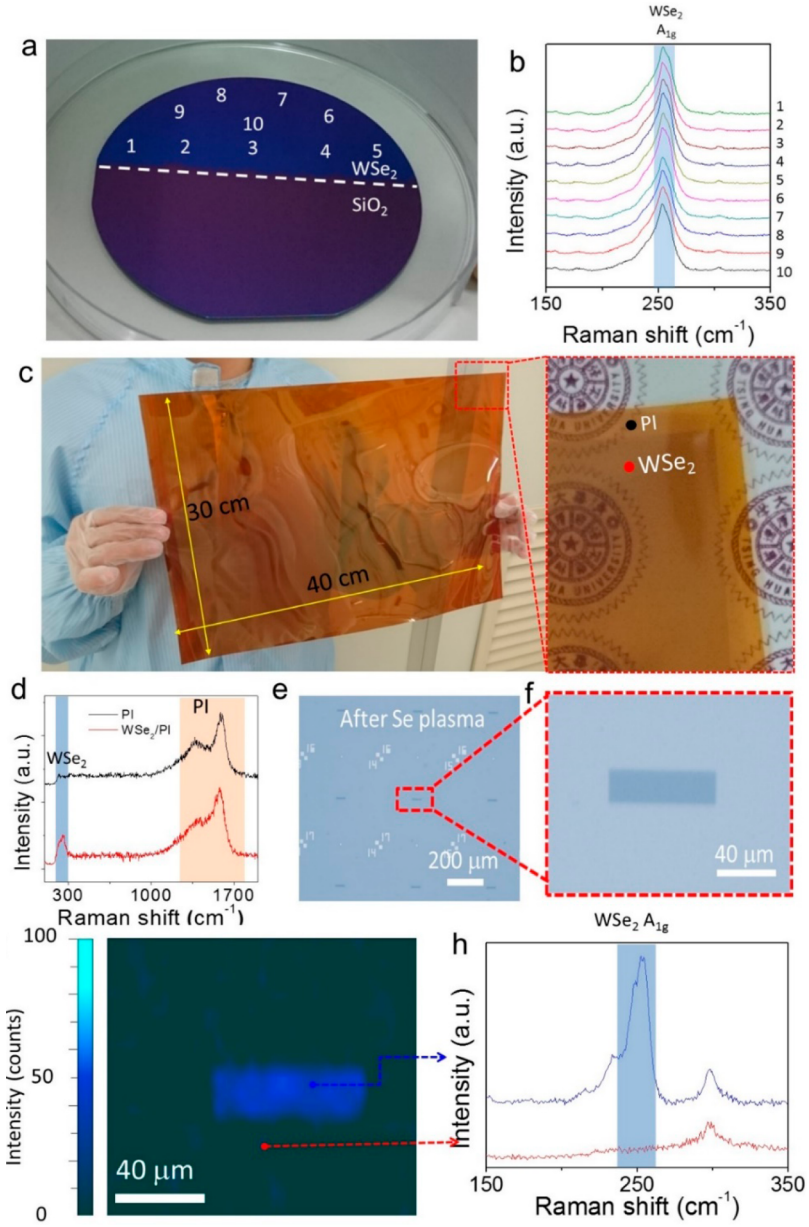

Figure 3. (a) Photographs of a few WSe_2 monolayers on half of a 4 in. SiO_x/Si wafer. (b) The corresponding Raman spectra at different positions in part a. (c) Photograph of a few WSe_2 monolayers on a 30 × 40 cm^2 polyimide flexible substrate at the plasma-assisted selenization temperature of 250 °C. The left inset is the magnified image of different contrasts between the polyimide flexible substrate and a few WSe_2 monolayers. (d) Raman spectra in part c, which correspond to the PI substrate (black spectra) and WSe_2 (red spectra). (e, f) OM images of patterning on a few WSe_2 monolayers after the plasma-assisted selenization of the WO_x film. (g) A Raman mapping image of patterning on a few WSe_2 monolayers. (h) The corresponding Raman spectrum of A_{1g} in part g.

including W^{6+} and W^{5+} oxidation states of WO_x ($A_{W4f7/2}$ + $A_{W4f5/2}$ + A_{W6+} + A_{W5+}). Obviously, the WSe_2 occurs in a pure H_2 environment. At a N:H_2 gas ratio of 2:1, the 30% conversion percentage of WSe_x can be found while 55% and 90% conversion percentages are reached with N_2:H_2 gas ratios of 1:1 and 1:2, respectively. No changes are observed in the Raman spectra under those conditions. However, in the pure H_2 environment, the broadened Raman peaks of WSe_2 with a strong background associated with damage in the substrate are observed (SiO_2 was used as a reference substrate for this test). A blue shift of W 4f spectra peaks under the higher H_2 ratio occurs, indicating a complete selenization of the W^{5+} oxidation state. Under the low H_2 atmosphere, the contribution of W^{6+} dominates, while the W^{5+} oxidation contributes to ~20% of the peak. On the basis of previously reported works, this value is in agreement with a stoichiometry of $WO_{2.9}$.[30] However, as the H_2 ratio increases, the contribution of W^{6+} is almost 100% for a stoichiometry closer to the crystalline WO_3. This result is opposite to the one expected from the expected reduction of WO_x into W metal.[31] This trend can be explained due to the lower Gibbs free energy of WO_3 (W^{6+} oxidation state) compared to other stoichiometries of WO_x (W^{5+} oxidation state).[32] Then, it is more reasonable to think that under a higher H_2 ratio the less stable WO_x (W^{5+} oxidation state) will be reduced to WSe_2 first.

One important advantage related to the synthesis of TMDs by the plasma-assisted selenization process is the possibility of depositing TMDs on arbitrary substrates, including SiO_2, glass,

DOI: 10.1021/acs.chemmater.6b04467
Chem. Mater. 2017, 29, 1587−1598

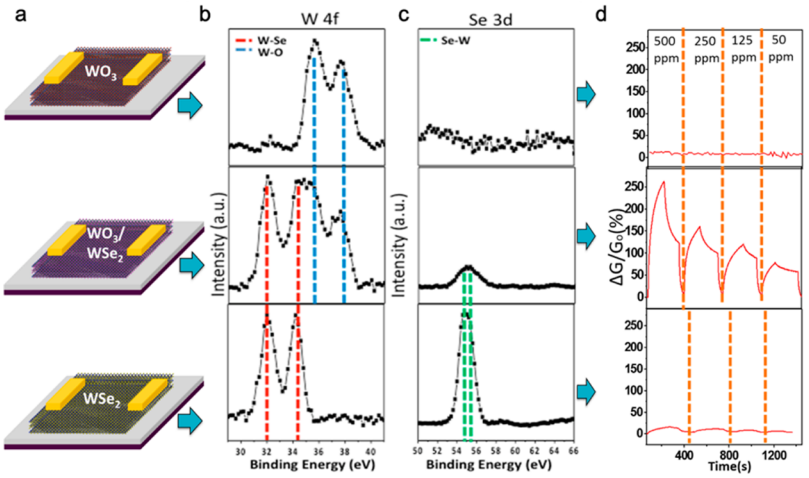

Figure 4. (a) Schematic diagram of the chemresistor configuration using WO_x, WO_x–WSe_2 hybrid, and WSe_2 films. In parts b and c, the W 4f and Se 3d XPS spectra are shown. In part d, the corresponding conductance changes upon NO gas exposure are shown.

and some high-temperature-resistant polymers, such as polyimide films. These substrates, in particular, are of special interest for several applications in transparent and flexible electronics. The large-area uniform growth of TMDs is still challenging, especially when following the CVD approach to TMD growth, which is limited by the size of the furnace tube. As a result, a vertical chamber design during the plasma-assisted selenization process allows the transformation of TMDs from metal oxides over a large area, which is exclusively restricted by the scalability of the chamber and sample holder. Figure 3a shows a photograph image of a few WSe_2 monolayers on a 300-nm-thick SiO_2/Si 4 in. wafer after the plasma-assisted selenization process, where WO_x was selectively deposited on a half wafer. The uniform dark blue color corresponds to WSe_2, and the purple area is the uncovered 300-nm-thick SiO_2 area. No major difference can be found on the 10 points marked from "1" to "10" within the WSe_2 region, as confirmed by Raman spectra, where the A_{1g} peak was measured as shown in Figure 3b. A photograph of a few WSe_2 monolayers formed on an 8 in. Si wafer, and the corresponding Raman spectra at different points confirm the potential of this process for formation over a large area and integration into CMOS technology (Figure S9). Furthermore, we directly demonstrated the growth of a few WSe_2 monolayers from 5-nm-thick WO_x film on a 30 × 40 cm^2 polyimide flexible substrate at the selenization temperature of 250 °C (Figure 3c). Note that the slight color difference can be observed on the polyimide flexible substrate (inset in Figure 3c), whose Raman spectra of two areas marked in the zoomed area in the inset of Figure 3c confirm the existence of the WSe_2 peak located at 250 cm^{-1} while no WSe_2 peak can be measured at the edge side of the polyimide flexible substrate (Figure 3d). Patentability is also fundamental for device fabrication. In a different way from the standard preparation of TMD devices that involves patterning of the device channel by dry etching, we predefine the channel areas during the deposition of the WO_x films using a standard photolithography method as shown in Figure 3e, where the gold markers were used as the alignment key. The corresponding magnified image is shown in Figure 3f. The A_{1g} Raman mapping image is shown in Figure 3g, which is taken from Figure 3f and shows similar color intensity, indicating the uniform formation of a few WSe_2 monolayers. The corresponding Raman spectra inside and outside the channel area confirm only the formation of a few WSe_2 monolayers from the predefined WO_x regions (Figure 3h).

The intrinsic p-type behavior of the plasma-assisted WSe_2 was further confirmed from the electrical characterization using a back gate configuration of fully selenized films as shown in Figure S10. Hall measurements were performed using a four-probe configuration to extract the intrinsic mobility of a few WSe_2 monolayers. The inset in Figure S11a shows an optical micrograph image of the Hall bar used for measurements with the current fixed at 1 nA. Figure S11a,b shows Hall resistance measurements in the formation of a few WSe_2 monolayers (~5 nm) from the WO_x films at selenization temperatures of 500 and 250 °C, which also confirms an intrinsic p-type behavior. The hole mobility (μ_{Hp}) can be calculated by $\mu_{Hp} = |V_H|/R_S IB = 1/(qn_sR_s)$, where B is the applied magnetic field, R_s is the sheet resistance, V_H is the Hall voltage, n_s is the carrier concentration, and q is the electron charge. Note that the Hall measurements were conducted in an open atmosphere. Interestingly, a few WSe_2 monolayers formed at the selenization temperature of 500 °C exhibit an intrinsic hole mobility of 40 $cm^2\ V^{-1}\ s^{-1}$, which is remarkably high compared to those of the other polycrystalline TMD monolayers synthesized at a similar temperature.[8,9] Interestingly, the hole mobility still maintains a relatively high hole mobility of approximately 6.4 $cm^2\ V^{-1}\ s^{-1}$ at the lowest selenization temperature of 250 °C.

As a gas sensor, some reports have shown excellent p-doping properties of WSe_2 under exposure of NO_x requiring annealing in order to achieve chemical bonding.[3] In this study, we aim to avoid chemical bonding in order to achieve only physical adsorption of the NO_x molecules for later desorption as a requirement for gas sensing devices. For a first NO_x sensor, we test three different samples with different conversion percentages between WO_3 to WSe_2 denoted as WO_3, WO_3/WSe_2, and WSe_2 (Figure 4). Figure 4a shows the schematic of the basic chemresistor device used for gas sensing while Figure 4b,c presents the XPS spectra of films. The corresponding conductance changes over time under exposure to different NO concentrations are measured in Figure 4d. In order to understand the response of the gas sensor, Figure S12 highlights the cycles used during the measurement as follows: At an initial state, the NO_x is first introduced in the chamber at the desired concentration and maintained for certain time (gas in). Second, the NO_x gas is pumped out of the chamber in

DOI: 10.1021/acs.chemmater.6b04467
Chem. Mater. 2017, 29, 1587–1598

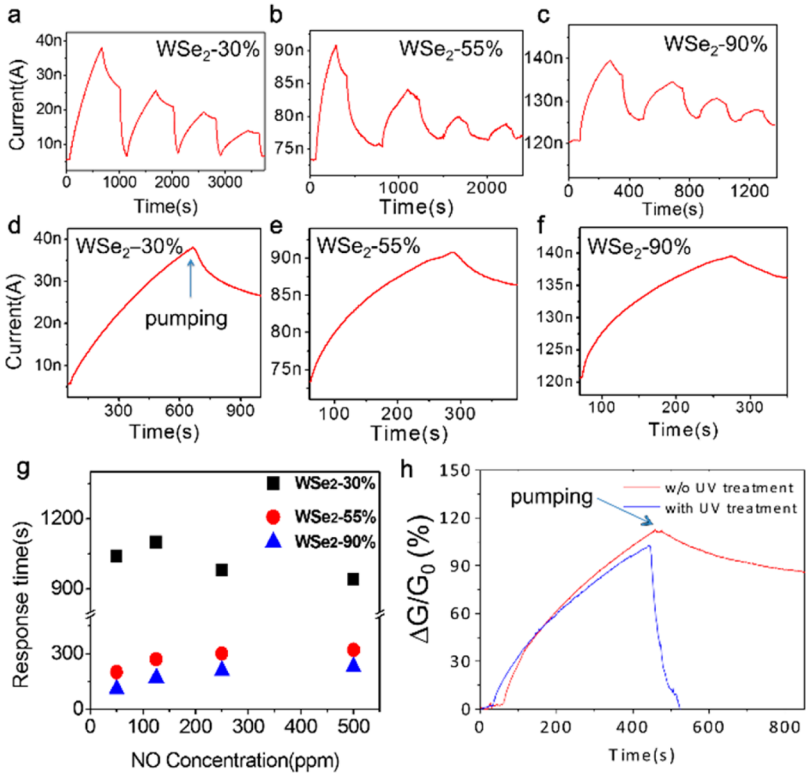

Figure 5. (a–c) Conductance variation after 500, 250, 125, and 50 ppm of NO gas exposure. (d–f) Adsorption and desorption conductance changes over time after exposure to 500 ppm of NO gas. (g) A summary plot of the adsorption response time (τ) and (h) comparison of desorption time with and without UV treatment.

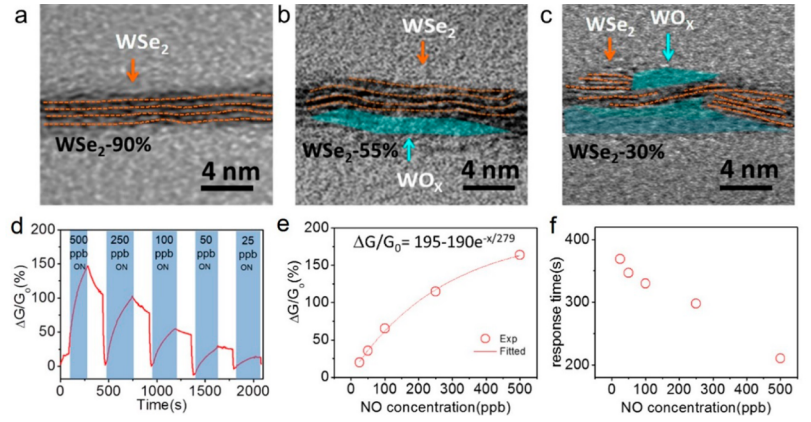

Figure 6. Cross-sectional TEM images of 7-nm-thick WO_x films exposed to the plasma power of 300 W with (a) 2:1, (b) 1:1, and (c) 1:2 H_2:N ratios at a selenization temperature of 250 °C. In parts c–e, the conductance variation after 500, 250, 125, 50, and 25 ppm of NO gas exposure. In parts d–f, adsorption and desorption conductance change over the time after exposure to 500 ppm of NO gas. (g) Summary plot of the adsorption response time (τ) and (h) comparison of desorption time with and without UV treatment.

order to desorb the gas from the surface of the gas sensor (gas out). Furthermore, in order to enhance the desorption process, a UV light was turned on (UV on). For a pure WO_x film, no response was obtained due to the poor crystallinity as a reference while the completely selenized WSe_2 sample was also tested, showing a minor response.

Interestingly, the device tested with a hybrid film mixing WO_x and WSe_2, namely, a half selenized film, exhibited a large sensitivity upon NO gas exposure compared with those of the pure WO_x and fully selenized WSe_2 samples (Figure 4d). The increased current is due to carrier transport from NO_x to WSe_2 since WSe_2 is the p-type material. Oxidizing gases (such as NO_x) extract electrons from the conduction band when adsorbed at the surface of a semiconductor, resulting in an increase of resistance for an n-type semiconductor (fewer electrons) while an increase in conductance will be noted in a p-type semiconductor (more holes).[33] The combination of different oxides to form hybrid heterojunctions such as SnO_x/WO_x offering a larger sensitivity for gas sensing than the pristine SnO_x and WO_x layers has also been demonstrated recently.[34] Despite that, several explanations have been employed; we believe that the large enhancement in sensitivity results from the carrier recombination in the local interface of "pn-junction" generated between WO_x and WSe_2 as schemati-

DOI: 10.1021/acs.chemmater.6b04467
Chem. Mater. 2017, 29, 1587–1598

cally constructed in Figure S13.[35,36] On the basis of those results, sensors fabricated with hybrid WO_x/WSe_2 films with different conversion percentages from 30% to 90% were measured in order to optimize the material ratio as presented in Figure 5. Considering WO_x as the n-type and WSe_2 as the p-type materials in the pn-junction, it is obvious to think that the ratio between the n- and p-type materials will influence the size of the depletion region at both sides of the pn-junction. Then, when the hybrid structure is dominated by the n-type semiconductor (WO_x), the depletion region will be enlarged in the p-type semiconductor (WSe_2). This enlargement of the depletion region induces a reduction of the free carriers in the p-type semiconductor, displaying a larger resistance as a base current (Figure 5a−c), thus increasing the sensitivity of the gas sensor. We do not discount that the presence of defect sites or Se vacancies caused by the plasma may enhance the sensitivity due to the higher chemical activity as suggested by other works.[37] Although the response time also increases with the sensitivity (Figure 5d−f and summarized in Figure 5g), the overall response is within a few minutes, which is acceptable for practical application in gas sensors. In addition, we found that a short UV treatment can enhance the desorption rate, reducing the total response time to less than 100 s in comparison to the several minutes required for self-detaching (Figure 5h).

The cross-section TEM images provide direct evidence of the coexistence of WO_x and WSe_2 at different conversion percentages (Figure 6a−c). As a result, a large junction interface generated between WO_x and WSe_2 can be observed for a WSe_2-30% hybrid film (Figure 6c). Furthermore, we focused on improving the desorption time, which is more critical than the adsorption time due to the long time required (5−6 times longer than the adsorption time). Several approaches have been tested on gas sensors in order to reduce the detaching time. Note that, with the increased WSe_2 concentration in the hybrid WO_x/WSe_2 films, the desorption is more difficult, and in many cases, the current cannot go back to the initial state similar to the results observed on MoS_2 sensors, which is due to the existence of WSe_2 edge sites, providing favorable Gibbs free energy to NO gas molecular adsorption compared to the basal plane.[38] However, we cannot prove this assumption from our experiments, and extra theoretical studies are required in the future. An additional test was carried out by increasing the operation temperature of the sensor (Figure S14). Although the detach rate can be enhanced, the sensitivity largely decreases. In all cases, the films showed good gas sensitivity compared with both WO_x and WSe_2, but in particular, the WSe_2-30% film exhibits an enhanced sensitivity over 280% at 50 ppm. Focusing on the WSe_2-30% film, we attempted to further reduce the NO concentration to ppb level. Figure 6d shows the response of the sensor in a range from 500 to 25 ppb. Furthermore, the electrical measurement at 25 ppb shows a noise signal smaller than 0.5% while reaching a sensitivity over 20% for a clear S/N of 40 (Figure S15). Similarly, the response to other NO concentrations was also fitted in a similar way to determine the maximum adsorption and response time as presented in Figure 6e,f. Obviously, the detection limit of our sensors is close to a value of 0.3 ppb at S/N larger than 10 from Figure 6d using an exponential fitting, which is an outstanding value for a gas sensor in a chemresistor configuration measured at room temperature. In a comparison of our results with other studies based on other materials, our results are comparable to the best (Table 2) with good stability and repeatability.

Table 2. Comparison of Other NO_x Gas Sensors Based on Other Materials

	method	sensitivity	limit of detection	response time	ref
MoS_2	mechanical exfoliation 2−3 layers	80%@3 ppm	0.8 ppm	~120 s	Hai Li et al.[38]
MoS_2-rGO + Pt	liquid exfoliation	15%@1.2 ppm	0.5 ppm	>30 min	Qiyuan He et al.[41]
Graphene	exfoliated	4%@1 ppm		within 1 min	Schedin et al.[42]
MoS_2	CVD	~20%@20 ppb		5−8 min	Bilu Liu et al.[43]
MoS_2	CVD	80%@120 ppb baseline@100 °C			Cho B. et al.[44]
black phosphorus	mechanical exfoliate	2.9%@5 ppb		280−350 s	Ahmad N. Abbas et al.[45]
hybrid WO_x/WSe_2	plasma-assisted selenization	~13%@25 ppb	estimated detection limit of 0.3 ppb@S/N > 10	~250 s	this work

DOI: 10.1021/acs.chemmater.6b04467
Chem. Mater. 2017, 29, 1587−1598

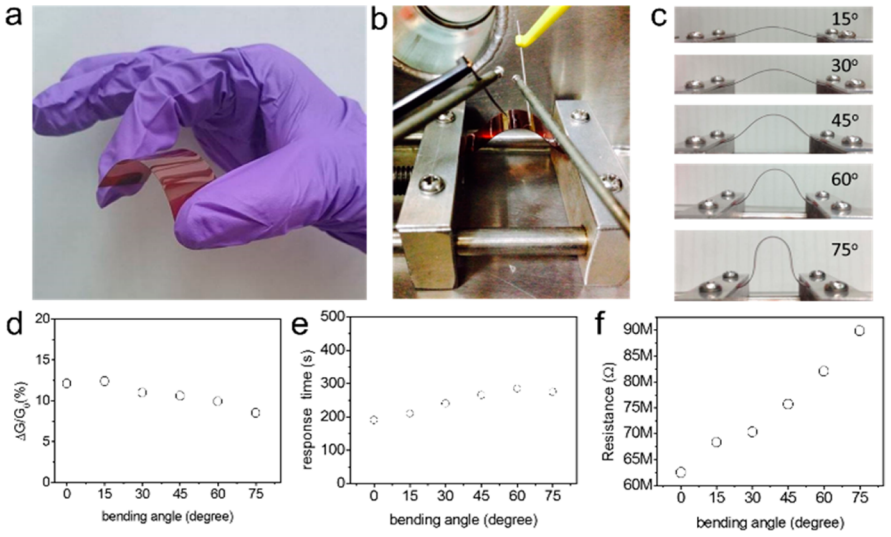

Figure 7. (a–c) Photographs of the gas sensor on a polymer substrate, the bending test device used during measurement, and the cross-sectional images of the device under different bending angles. (d–f) Sensitivity, response time, and film resistance under different bending angles, respectively.

Furthermore, the development of sensors on flexible substrates for wearable electronics is becoming an important area of research.[39,40] For that reason, we also prepared the devices directly on flexible substrates (polyimide) for a bending test as shown in Figure 7a. The experimental setup for the electrical measurement during bending is displayed in Figure 7b. Figure 7c displays the different angles used for the measurements. The corresponding $\Delta G/G_0$, response time, and resistance were recorded in Figure 7d–f, respectively. For bending angles >45°, a slight decrease in the sensitivity was observed. At the larger bending angles, a more pronounced decrease in the sensitivity is found. However, the devices remain operational even at the large bending angle of 75°. Note that a clear change in the film resistance was measured. However, this variation is rather small compared with the conductance change upon exposure to NO gas. These findings indicate that our low-temperature plasma-assisted selenization process provides a pathway to the direct formation of large-area TMD films on plastic substrates. In addition to the plasma-assisted selenization process for the formation of MSe_2-based TMDs at an extremely low temperature, we believe that the current design for the plasma treatment can also be applied to different "reduction" processes of metal oxides, such as plasma-assisted sulfurization and telluridization processes, which will open a new window for the formation of versatile TMDs for integration with existing technologies that require lower process temperatures and maintain a manageable thermal budget. The process can also be compatible with other semiconductor processes, which will be desirable for technology development in the next generation of applications.

CONCLUSION

In summary, we have demonstrated the growth of TMDs at low temperatures, as low as 250 °C using the plasma-assisted selenization process applied to metal oxides. Two types of TMDs, WSe_2 and $MoSe_2$, which are converted from WO_x and MoO_x films, were demonstrated at a formation temperature as low as 250 °C. To demonstrate the plasma-assisted selenization at low temperatures, optimization of the growth parameters through the formation of a few WSe_2 monolayers as the model material system was chosen due to its technological importance as a p-type inorganic semiconductor with an excellent hole mobility and good adsorption of NO_x molecules. FET devices made of a few WSe_2 monolayers show evidence for the p-type behavior. Processing at temperatures of 500 and 250 °C exhibited the hole mobility of ~40 and ~6 $cm^2\ V^{-1}\ s^{-1}$ with plasma powers of 50 and 400 W. Additionally, a large-area synthesis of WSe_2 on a polyimide (30 × 40 cm^2) flexible substrate and 8 in. silicon wafer with good uniformity was demonstrated, thus creating a suitable process for future industrial development on flexible and wearable electronics. With control of the different ratios of forming gas between N_2 and H_2 gases, a 5-nm-thick WO_x/WSe_2 hybrid structure possessing a high sensitivity to NO_x of over 20% at only 25 ppb with a S/N ratio over 10 operating at room temperature and an estimated detection limit up to 0.3 ppb at a S/N ratio >10 has been demonstrated. Our hybrid films with a thickness of a few nanometers show high sensitivity measured at room temperature and the potential for a low-temperature process for direct deposition on plastic substrates for plastic and wearable electronics. Most importantly, the low-temperature plasma-assisted selenization process can be extended to the synthesis of other chalcogenide materials at low temperatures, which would allow the integration of TMD materials with existing technologies that require lower process temperatures and maintain a manageable thermal budget.

ASSOCIATED CONTENT

Supporting Information

The Supporting Information is available free of charge on the ACS Publications website at DOI: 10.1021/acs.chemmater.6b04467.

Additional details of the system and additional characterization details (PDF)

AUTHOR INFORMATION

Corresponding Author

*E-mail: ylchueh@mx.nthu.edu.tw.

ORCID

Kang L. Wang: 0000-0002-7439-6920

Yu-Lun Chueh: 0000-0002-0155-9987

DOI: 10.1021/acs.chemmater.6b04467
Chem. Mater. 2017, 29, 1587–1598

Notes

The authors declare no competing financial interest.

■ ACKNOWLEDGMENTS

The research is supported by the Ministry of Science and Technology through Grants 105-3113-E-007-003-CC2, 104-2628-M-007-004-MY3, 104-2221-E-007-048-MY3, 105-2633-M-007-003, and 104-2622-M-007-002-CC2 and the National Tsing Hua University through Grant 105A0088J4. Y.-L.C. greatly appreciates the use of the facility at CNMM.

■ REFERENCES

(1) Thomas, S. R.; Pattanasattayavong, P.; Anthopoulos, T. D. Solution-processable metal oxide semiconductors for thin-film transistor applications. *Chem. Soc. Rev.* **2013**, *42* (16), 6910−6923.

(2) Fortunato, E.; Barquinha, P.; Martins, R. Oxide semiconductor thin-film transistors: a review of recent advances. *Adv. Mater.* **2012**, *24* (22), 2945−2986.

(3) Zhao, P.; Kiriya, D.; Azcatl, A.; Zhang, C.; Tosun, M.; Liu, Y. S.; Hettick, M.; Kang, J. S.; McDonnell, S.; Santosh, K. C.; Guo, J.; Cho, K.; Wallace, R. M.; Javey, A. Air stable p-doping of WSe2 by covalent functionalization. *ACS Nano* **2014**, *8* (10), 10808−10814.

(4) Huang, J. K.; Pu, J.; Hsu, C. L.; Chiu, M. H.; Juang, Z. Y.; Chang, Y. H.; Chang, W. H.; Iwasa, Y.; Takenobu, T.; Li, L. J. Large-area synthesis of highly crystalline WSe2 monolayers and device applications. *ACS Nano* **2014**, *8* (1), 923−930.

(5) Zhou, H.; Wang, C.; Shaw, J. C.; Cheng, R.; Chen, Y.; Huang, X.; Liu, Y.; Weiss, N. O.; Lin, Z.; Huang, Y.; Duan, X. Large area growth and electrical properties of p-type WSe2 atomic layers. *Nano Lett.* **2015**, *15* (1), 709−713.

(6) Huang, J.; Yang, L.; Liu, D.; Chen, J.; Fu, Q.; Xiong, Y.; Lin, F.; Xiang, B. Large-area synthesis of monolayer WSe2 on a SiO2/Si substrate and its device applications. *Nanoscale* **2015**, *7* (9), 4193−4198.

(7) Chen, J.; Liu, B.; Liu, Y.; Tang, W.; Nai, C. T.; Li, L.; Zheng, J.; Gao, L.; Zheng, Y.; Shin, H. S.; Jeong, H. Y.; Loh, K. P. Chemical Vapor Deposition of Large-Sized Hexagonal WSe Crystals on Dielectric Substrates. *Adv. Mater.* **2015**, *27*, 6722−6727.

(8) Kang, K.; Xie, S.; Huang, L.; Han, Y.; Huang, P. Y.; Mak, K. F.; Kim, C. J.; Muller, D.; Park, J. High-mobility three-atom-thick semiconducting films with wafer-scale homogeneity. *Nature* **2015**, *520* (7549), 656−660.

(9) Gong, Y.; Lin, Z.; Ye, G.; Shi, G.; Feng, S.; Lei, Y.; Elias, A. L.; Perea-Lopez, N.; Vajtai, R.; Terrones, H.; Liu, Z.; Terrones, M.; Ajayan, P. M. Tellurium-Assisted Low-Temperature Synthesis of MoS and WS Monolayers. *ACS Nano* **2015**, *9* (12), 11658−11666.

(10) Browning, P.; Eichfeld, S.; Zhang, K.; Hossain, L.; Lin, Y.-C.; Wang, K.; Lu, N.; Waite, A. R.; Voevodin, A. A.; Kim, M.; Robinson, J. A. Large-area synthesis of WSe2 from WO3by selenium−oxygen ion exchange. *2D Mater.* **2015**, *2* (1), 014003.

(11) Lin, Y.-C.; Lu, C.-C.; Yeh, C.-H.; Jin, C.; Suenaga, K.; Chiu, P.-W. Graphene Annealing: How Clean Can It Be? *Nano Lett.* **2012**, *12* (1), 414−419.

(12) Pradhan, N. R.; Rhodes, D.; Memaran, S.; Poumirol, J. M.; Smirnov, D.; Talapatra, S.; Feng, S.; Perea-Lopez, N.; Elias, A. L.; Terrones, M.; Ajayan, P. M.; Balicas, L. Hall and field-effect mobilities in few layered p-WSe2 field-effect transistors. *Sci. Rep.* **2015**, *5*, 8979.

(13) Chen, L.; Liu, B.; Ge, M.; Ma, Y.; Abbas, A. N.; Zhou, C. Step-Edge-Guided Nucleation and Growth of Aligned WSe2 on Sapphire via a Layer-over-Layer Growth Mode. *ACS Nano* **2015**, *9* (8), 8368−75.

(14) Li, H.; Wu, H.; Yuan, S.; Qian, H. Synthesis and characterization of vertically standing MoS_2 nanosheets. *Sci. Rep.* **2016**, *6*, 21171.

(15) Terrones, H.; Del Corro, E.; Feng, S.; Poumirol, J. M.; Rhodes, D.; Smirnov, D.; Pradhan, N. R.; Lin, Z.; Nguyen, M. A.; Elias, A. L.; Mallouk, T. E.; Balicas, L.; Pimenta, M. A.; Terrones, M. New first order Raman-active modes in few layered transition metal dichalcogenides. *Sci. Rep.* **2014**, *4*, 4215.

(16) Zhao, W.; Ghorannevis, Z.; Amara, K. K.; Pang, J. R.; Toh, M.; Zhang, X.; Kloc, C.; Tan, P. H.; Eda, G. Lattice dynamics in mono- and few-layer sheets of WS2 and WSe2. *Nanoscale* **2013**, *5* (20), 9677−83.

(17) Chen, Y. Z.; Medina, H.; Su, T. Y.; Li, J. G.; Cheng, K. Y.; Chiu, P. W.; Chueh, Y. L. Ultrafast and low temperature synthesis of highly crystalline and patternable few-layers tungsten diselenide by laser irradiation assisted selenization process. *ACS Nano* **2015**, *9* (4), 4346−4353.

(18) Masuzawa, T.; Saito, I.; Yamada, T.; Onishi, M.; Yamaguchi, H.; Suzuki, Y.; Oonuki, K.; Kato, N.; Ogawa, S.; Takakuwa, Y.; Koh, A. T.; Chua, D. H.; Mori, Y.; Shimosawa, T.; Okano, K. Development of an amorphous selenium-based photodetector driven by a diamond cold cathode. *Sensors* **2013**, *13* (10), 13744−13778.

(19) Yamamoto, M.; Dutta, S.; Aikawa, S.; Nakaharai, S.; Wakabayashi, K.; Fuhrer, M. S.; Ueno, K.; Tsukagoshi, K. Self-limiting layer-by-layer oxidation of atomically thin WSe2. *Nano Lett.* **2015**, *15* (3), 2067−2073.

(20) Wang, X.; Gong, Y.; Shi, G.; Chow, W. L.; Keyshar, K.; Ye, G.; Vajtai, R.; Lou, J.; Liu, Z.; Ringe, E.; Tay, B. K.; Ajayan, P. M. Chemical Vapor Deposition Growth of Crystalline Monolayer MoSe2. *ACS Nano* **2014**, *8* (5), 5125−5131.

(21) Chang, Y. H.; Zhang, W.; Zhu, Y.; Han, Y.; Pu, J.; Chang, J. K.; Hsu, W. T.; Huang, J. K.; Hsu, C. L.; Chiu, M. H.; Takenobu, T.; Li, H.; Wu, C. I.; Chang, W. H.; Wee, A. T.; Li, L. J. Monolayer MoSe2 grown by chemical vapor deposition for fast photodetection. *ACS Nano* **2014**, *8* (8), 8582−8590.

(22) Azcatl, A.; Kc, S.; Peng, X.; Lu, N.; McDonnell, S.; Qin, X.; de Dios, F.; Addou, R.; Kim, J.; Kim, M. J.; Cho, K.; Wallace, R. M. HfO2on UV−O3exposed transition metal dichalcogenides: interfacial reactions study. *2D Mater.* **2015**, *2* (1), 014004.

(23) Medina, H.; Lin, Y.-C.; Jin, C.; Lu, C.-C.; Yeh, C.-H.; Huang, K.-P.; Suenaga, K.; Robertson, J.; Chiu, P.-W. Metal-Free Growth of Nanographene on Silicon Oxides for Transparent Conducting Applications. *Adv. Funct. Mater.* **2012**, *22* (10), 2123−2128.

(24) Duan, X.; Wang, C.; Shaw, J. C.; Cheng, R.; Chen, Y.; Li, H.; Wu, X.; Tang, Y.; Zhang, Q.; Pan, A.; Jiang, J.; Yu, R.; Huang, Y.; Duan, X. Lateral epitaxial growth of two-dimensional layered semiconductor heterojunctions. *Nat. Nanotechnol.* **2014**, *9* (12), 1024−1030.

(25) Malm, J.; Sajavaara, T.; Karppinen, M. Atomic Layer Deposition of WO3 Thin Films using W(CO)6 and O3 Precursors. *Chem. Vap. Deposition* **2012**, *18* (7−9), 245−248.

(26) Li, G.; Varga, T.; Yan, P.; Wang, Z.; Wang, C.; Chambers, S. A.; Du, Y. Crystallographic dependence of photocatalytic activity of WO3 thin films prepared by molecular beam epitaxy. *Phys. Chem. Chem. Phys.* **2015**, *17* (23), 15119−15123.

(27) Fang, G. J.; Liu, Z. L.; Sun, G. C.; Yao, K. L. Preparation and Electrochromic Properties of Nanocrystalline WO3 Thin Films Prepared by Pulsed Excimer Laser Ablation Technique. *Phys. Status Solidi A* **2001**, *184* (1), 129−137.

(28) De Angelis, B. A.; Schiavello, M. X-ray photoelectron spectroscopy study of nonstoichiometric tungsten oxides. *J. Solid State Chem.* **1977**, *21* (1), 67−72.

(29) Kong, D.; Cha, J. J.; Lai, K.; Peng, H.; Analytis, J. G.; Meister, S.; Chen, Y.; Zhang, H. J.; Fisher, I. R.; Shen, Z. X.; Cui, Y. Rapid surface oxidation as a source of surface degradation factor for Bi(2)Se(3). *ACS Nano* **2011**, *5* (6), 4698−703.

(30) Senthil, K.; Yong, K. Growth and characterization of stoichiometric tungsten oxide nanorods by thermal evaporation and subsequent annealing. *Nanotechnology* **2007**, *18* (39), 395604.

(31) Xie, F. Y.; Gong, L.; Liu, X.; Tao, Y. T.; Zhang, W. H.; Chen, S. H.; Meng, H.; Chen, J. XPS studies on surface reduction of tungsten oxide nanowire film by Ar+ bombardment. *J. Electron Spectrosc. Relat. Phenom.* **2012**, *185* (3−4), 112−118.

(32) Sha, L.; Qiu, Z. J. Thermodynamic calculation on reduction of tungsten oxide in H2 atm. *Int. J. Refract. Hard Met.* **2008**, *26* (4), 362−366.

DOI: 10.1021/acs.chemmater.6b04467
Chem. Mater. 2017, 29, 1587−1598

(33) Wisitsoraat, A.; Tuantranont, A.; Comini, E.; Sberveglieri, G.; Wlodarski, W. Characterization of n-type and p-type semiconductor gas sensors based on NiOx doped TiO2 thin films. *Thin Solid Films* **2009**, *517* (8), 2775−2780.
(34) Miller, D. R.; Akbar, S. A.; Morris, P. A. Nanoscale metal oxide-based heterojunctions for gas sensing: A review. *Sens. Actuators, B* **2014**, *204*, 250−272.
(35) Weinhardt, L.; Blum, M.; Bär, M.; Heske, C.; Cole, B.; Marsen, B.; Miller, E. L. Electronic Surface Level Positions of WO3Thin Films for Photoelectrochemical Hydrogen Production. *J. Phys. Chem. C* **2008**, *112* (8), 3078−3082.
(36) Kang, J.; Tongay, S.; Zhou, J.; Li, J.; Wu, J. Band offsets and heterostructures of two-dimensional semiconductors. *Appl. Phys. Lett.* **2013**, *102* (1), 012111.
(37) Qu, Y.; Medina, H.; Wang, S. W.; Wang, Y. C.; Chen, C. W.; Su, T. Y.; Manikandan, A.; Wang, K.; Shih, Y. C.; Chang, J. W.; Kuo, H. C.; Lee, C. Y.; Lu, S. Y.; Shen, G.; Wang, Z. M.; Chueh, Y. L. Wafer Scale Phase-Engineered 1T- and 2H-MoSe2 /Mo Core-Shell 3D-Hierarchical Nanostructures toward Efficient Electrocatalytic Hydrogen Evolution Reaction. *Adv. Mater.* **2016**, *28*, 9831−9838.
(38) Li, H.; Yin, Z.; He, Q.; Li, H.; Huang, X.; Lu, G.; Fam, D. W.; Tok, A. I.; Zhang, Q.; Zhang, H. Fabrication of single- and multilayer MoS2 film-based field-effect transistors for sensing NO at room temperature. *Small* **2012**, *8* (1), 63−67.
(39) Kim, J.; Lee, M. S.; Jeon, S.; Kim, M.; Kim, S.; Kim, K.; Bien, F.; Hong, S. Y.; Park, J. U. Highly transparent and stretchable field-effect transistor sensors using graphene-nanowire hybrid nanostructures. *Adv. Mater.* **2015**, *27* (21), 3292−3297.
(40) Park, J.; Kim, J.; Kim, K.; Kim, S. Y.; Cheong, W. H.; Park, K.; Song, J. H.; Namgoong, G.; Kim, J. J.; Heo, J.; Bien, F.; Park, J. U. Wearable, wireless gas sensors using highly stretchable and transparent structures of nanowires and graphene. *Nanoscale* **2016**, *8* (20), 10591−10597.
(41) He, Q.; Zeng, Z.; Yin, Z.; Li, H.; Wu, S.; Huang, X.; Zhang, H. Fabrication of flexible MoS2 thin-film transistor arrays for practical gas-sensing applications. *Small* **2012**, *8* (19), 2994−2999.
(42) Schedin, F.; Geim, A. K.; Morozov, S. V.; Hill, E. W.; Blake, P.; Katsnelson, M. I.; Novoselov, K. S. Detection of individual gas molecules adsorbed on graphene. *Nat. Mater.* **2007**, *6* (9), 652−655.
(43) Liu, B.; Chen, L.; Liu, G.; Abbas, A. N.; Fathi, M.; Zhou, C. High-performance chemical sensing using Schottky-contacted chemical vapor deposition grown monolayer MoS2 transistors. *ACS Nano* **2014**, *8* (5), 5304−5314.
(44) Cho, B.; Kim, A. R.; Park, Y.; Yoon, J.; Lee, Y. J.; Lee, S.; Yoo, T. J.; Kang, C. G.; Lee, B. H.; Ko, H. C.; Kim, D. H.; Hahm, M. G. Bifunctional sensing characteristics of chemical vapor deposition synthesized atomic-layered MoS2. *ACS Appl. Mater. Interfaces* **2015**, *7* (4), 2952−2959.
(45) Abbas, A. N.; Liu, B.; Chen, L.; Ma, Y.; Cong, S.; Aroonyadet, N.; Kopf, M.; Nilges, T.; Zhou, C. Black phosphorus gas sensors. *ACS Nano* **2015**, *9* (5), 5618−5624.

DOI: 10.1021/acs.chemmater.6b04467
Chem. Mater. 2017, 29, 1587−1598